Asian Journal of Chemistry; Vol. 34, No. 7 (2022), 1863-1868

ASIAN JOURNAL OF CHEMISTRY

https://doi.org/10.14233/ajchem.2022.23621

First Principle DFT + U Calculations for the Optoelectronic Properties of Cu and C-Cu co-doped TiO_2 Anatase Model

F. ULLAH[1,2,3], N.M. MOHAMED[1,2], U. GHANI[4] and M.S.M. SAHEED[2,5,*]

[1]Department of Fundamental and Applied Sciences, Universiti Teknologi PETRONAS, 32610 Bandar Seri Iskandar, Perak, Malaysia
[2]Centre of Innovative Nanostructure and Nanodevices (COINN), Universiti Teknologi PETRONAS, 32610 Bandar Seri Iskandar, Perak, Malaysia
[3]Department of Physics, University of Science and Technology, Bannu 28100, Khyber Pakhtunkhwa, Pakistan
[4]State Key Laboratory of Metal Matrix Composites, Shanghai Jiao Tong University, Shanghai 200240, P.R. China
[5]Department of Mechanical Engineering, Universiti Teknologi PETRONAS, 32610 Seri Iskandar, Perak Darul Ridzuan, Malaysia

*Corresponding author: E-mail: shuaib.saheed@utp.edu.my

Received: 14 November 2021; *Accepted*: 23 May 2022; *Published online*: 15 June 2022; AJC-20867

The metal-cations and non-metal anions mono-doped titanium dioxide (TiO_2) systems have shown limited success as an efficient photocatalyst for various photocatalytic applications. Instead, the co-doping of TiO_2 with metal and non-metal dopants is transpired as an effective doping approach to reduce the wide bandgap of the TiO_2 and harvest a greater amount of the visible solar spectrum. Herein, a computational study was systematically performed to develop an efficient carbon-copper (C-Cu) co-doped TiO_2 anatase system and compared its optoelectronic characteristics with the copper (Cu) mono-doped TiO_2 system. The structural properties simulated with Perdew–Burke–Ernzerhof assisted generalized gradient approximation (GGA + PBE) whereas the electronic and optical properties with Hubbard's modified (GGA + U) approximation. The electronic band structure and density of states plots display reduced bandgap energy of 2.30 eV for the C-Cu co-doped TiO_2 anatase model in comparison to Cu mono-doped TiO_2 anatase model. Moreover, the absorption spectra display a redshift of the optical absorption edge up to 515 nm for the co-doped system. Overall, the DFT work provide clear insights and predictions that the C-Cu co-doped TiO_2 anatase model has an efficient bandgap narrowing with a significant redshift of the optical absorption edge in comparison to Cu mono-doped TiO_2 model.

Keywords: Anatase TiO_2, Doping, Density functional theory, Bandgap reduction, Optical absorption.

INTRODUCTION

Direct harvesting of solar light and its conversion into chemical energy by photoelectrochemical solar hydrogen production is presumed to be a cleaner renewable energy approach to take up the serious issues related to the energy crisis and environmental challenges [1]. Semiconductor photocatalysts provide an easy way for the utilization of solar energy and thus play an important role in photocatalytic water-splitting hydrogen evaluation techniques. Titanium dioxide (TiO_2) is considered great attention as a popular photocatalytic material due to its suitable band edge positions for water splitting, low cost, availability and chemical stability [2-4]. However, single component TiO_2 photocatalyst have insufficient solar energy applications due to their wide bandgap (3.2 eV for anatase TiO_2) and high recombination rate of photoinduced charge carriers [5]. Due to these reasons, TiO_2 mostly endure from poor photocatalytic activity under the solar spectrum, as it absorbs only ultraviolet (UV) radiations (3-5%) of the solar spectrum. The efficient utilization of solar energy is therefore too much important to promote the oxidation/reduction reactions on the surface of the photocatalyst [5,6]. Many approaches including metal and non-metal mono-doping have been examined to enhance the optical absorption of TiO_2 in the visible array of the solar spectra, by introducing the impurity energy states in the valance band (VB) [7,8] and conduction band (CB) regions of TiO_2 photocatalyst. The induced impurity states thus reduced the bandgap energy and hence improved the visible light absorption. TiO_2 doping with numerous metal dopants including Cu, Pt, *etc.* and nonmetals C, N, B and S, *etc.* [4,6-8] have been

This is an open access journal, and articles are distributed under the terms of the Attribution 4.0 International (CC BY 4.0) License. This license lets others distribute, remix, tweak, and build upon your work, even commercially, as long as they credit the author for the original creation. You must give appropriate credit, provide a link to the license, and indicate if changes were made.

reported to modify the optoelectronic characteristics of host crystal structure. Researchers predict that the bandgap reduction of TiO_2 anatase model with an enhanced redshift in the optical absorption spectra (to use the wide spectral region of the solar irradiation) will thus improve the visible light photocatalytic activity. Although, metal and non-metal doping techniques illustrate better performance for solar hydrogen production in comparison to undoped TiO_2. However, these techniques still provide limited success in improving the photocatalytic performance of the modified photocatalyst [9-13].

On the other hand, the metal-non-metal co-doping reduces the bandgap energy of TiO_2 to an optimal range and has been reported both theoretically and experimentally to be a more effective approach than metal and non-metal mono-doping. In comparison to undoped and mono-doped TiO_2, the co-doped TiO_2 photocatalysts have great potential in solar energy applications and demonstrate enhanced photocatalytic performance for solar hydrogen evaluation. Yun *et al.* [10] reported the carbon, nitrogen (C, N) co-doped TiO_2 rutile model *via* DFT calculation using plane-wave pseudopotential approach and concluded that the C-N co-doped TiO_2 rutile model displays better visible light absorption than C/N mono-doped TiO_2. Dan *et al.* [9] suggested that the replacement of two O atoms with two N atoms greatly enhances visible light absorption. The induced impurity states due to the coupling between O2p and C2p states reduced the bandgap energy and thus led to the redshift of optical absorption edge. They claimed an obviously increased efficiency of visible light absorption after co-doping. The photocatalytic performance of the co-doped TiO_2 systems can further be improved by properly choosing the dopant materials and deeply understanding the photocatalytic mechanism at the nanoscale [14]. Several factors, involving the distribution of impurity levels, the bandgap energy and the Fermi level of co-doped TiO_2 influence the performance of co-doped TiO_2 predominantly. Computational simulation *via* DFT calculations might predict many photocatalytic characteristics of the various materials and choose the suitable one for practical purposes [10]. Notably, mostly reported theoretical works reported the conventional DFT calculation approaches for the bandgap energy calculations of doped TiO_2 models [8,10,13].

Herein, the present work examined the effect of Cu mono-doping and C-Cu co-doping on the structural, electronic and optical characteristics of TiO_2 anatase model by employing Hubbard's framed DFT calculations. The structural properties of all the designed models were investigated *via* GGA + PBE whereas, the electronic and optical properties were examined through GGA + U functional approach. The band structure and density of states analysis of C-Cu co-doped TiO_2 model confirmed a significant bandgap reduction up to 2.30 eV and improved visible light absorption in comparison to the undoped TiO_2 anatase model.

COMPUTATIONAL METHODS

All the computational simulation for the present study has been done with the Cambridge sequential total energy package (CASTEP) code within the Materials Studio software. The CASTEP code is based upon the DFT approach with the total energy plane-wave pseudo-potential approach to the valence electron states within a plane-wave basis set [10]. Initially, the geometric structures of the designed models have been optimized. The structural properties were computed through GGA + PBE exchange correlational functional whereas, the GGA + U scheme was employed for the electronic and optical properties calculations. The conventional GGA + PBE exchange correlational functional generally underestimates the bandgap energies of the transition metal oxides as it does not designate the strong Coulomb interactions precisely for the electrons of *d*- and/or *f*-orbitals [11,12]. On the other hand, the GGA + U potential has been reported to yield more accurate results for the electronic structure and optical properties by estimating strongly correlated interactions in the *d*- and *f*-orbitals through an on-site Coulomb's correction term and therefore, the approach is widely adopted to define the systems more accurately with localized *d*- and *f*-electrons [13,14]. Various values of the U parameter were employed to the valence Ti 3*d*-electrons to obtain the accurate bandgap energy value that is much closer to the experimental values. The value of U ~ 8.47 eV was thus taken for the TiO_2 based model. Furthermore, the Hubbard's modified DFT technique offers a decent balance out between the available computational resources and the accuracy of the computed results [15].

The Cu-doped TiO_2 anatase $2 \times 3 \times 1$ supercell model was built by substituting a Ti atom with Cu atom in the undoped TiO_2 supercell model and simulate the optoelectronic properties of Cu-doped TiO_2 anatase system. For C-Cu co-doped TiO_2 anatase system, the simulation was conducted for the said $2 \times 3 \times 1$ optimized undoped TiO_2 anatase supercell by substituting an O atom with C and Ti atom with Cu atom. The atomic positions and cell parameters of the designed models were optimized with residual forces below 0.03 eV/Å. The ultra-soft pseudopotential functional was adopted to accelerate the computational runs and employed to the electronic configuration of Ti; $3s^2\ 3p^6\ 3d^2\ 4s^2$, O; $2s^2\ 2p^4$, C; $2s^2\ 2p^2$ and Cu; $3d^{10}\ 4s^1$.

A $4 \times 4 \times 4$ Monkhorst-Pack k-point mesh over the Brillouin zone was chosen for numerical sampling integration. The convergence parameters were specified with the cutoff energy of about 380 eV for the valence electrons wave-function, the stress on the atom less than 0.1 GPa, the self-consistent field (SCF) iterations convergence threshold limited below 2×10^{-4} eV/atom and the atomic displacement equal to 2×10^{-3} Å. The settings of these necessary parameters produce sufficient distinct features to analyze the various optoelectronic characteristics like electronic band structure, total density of states (TDOS), partial density of states (PDOS) as well as the optical absorption spectra.

RESULTS AND DISCUSSION

Structural properties: The TiO_2 anatase lattice structure preserves a tetragonal geometry unit structure, belongs to $I4_1/amd$ symmetry space group. The unit cell contains four TiO_2 units, with Ti atoms positioned in slightly distorted octahedral symmetry whereas O atoms are positioned in a Y-shaped tri-

coordinated geometry, as reported in our previous work. The computed lattice parameters for the undoped TiO_2 unit cell model were a = 3.776 Å, b = 3.776 Å and c = 9.486 Å, as reported earlier [12] and matched well with the experimental values of the TiO_2 anatase $a = b$ = 3.785 Å and c = 9.539 Å [10] and thus indicates that the adopted simulation technique is reliable. It is notable to mention that the calculated lattice parameter value of the c-axis is around 9.486 Å, almost 2.5 times more than the a- and b-axes (3.776 Å), which may result in a significant anisotropy of the material's properties. The computationally generated DFT simulation images for the TiO_2 anatase unit cell in real space, in primitive configuration and in reciprocal space is shown in Fig. 1.

To design various doped models, initially, the 2 × 3 × 1 TiO_2 supercell model was designed that including a total of 117 atoms with 39 Ti and 78 O atoms. The concept of supercell approach was employed to the undoped TiO_2 system to effectively adjust the dopant atoms into the TiO_2 system. Moreover, the supercell model effectually represents a bulk solid even though by simulating a comparatively small block (supercell) of the TiO_2 model. It was also reported in the literature fluently that the supercell modeling approach effectively employed to display a non-periodic entity such as a vacancy *etc.* present in the system [16].

Cu-doped TiO_2 model was designed by replacing a Ti atom with Cu atom in the undoped TiO_2 supercell, as demonstrated in Fig. 2a. The designed Cu-doped model also has a total of 117 atoms with 38 Ti, 1 Cu and 78 O atoms. The structural modifications were observed because of the incorporation of dopant entities that altered the lattice parameters of undoped TiO_2 lattice as shown in Table-1. The C-Cu co-doped TiO_2 supercell was designed by replacing an O atom with C and Ti

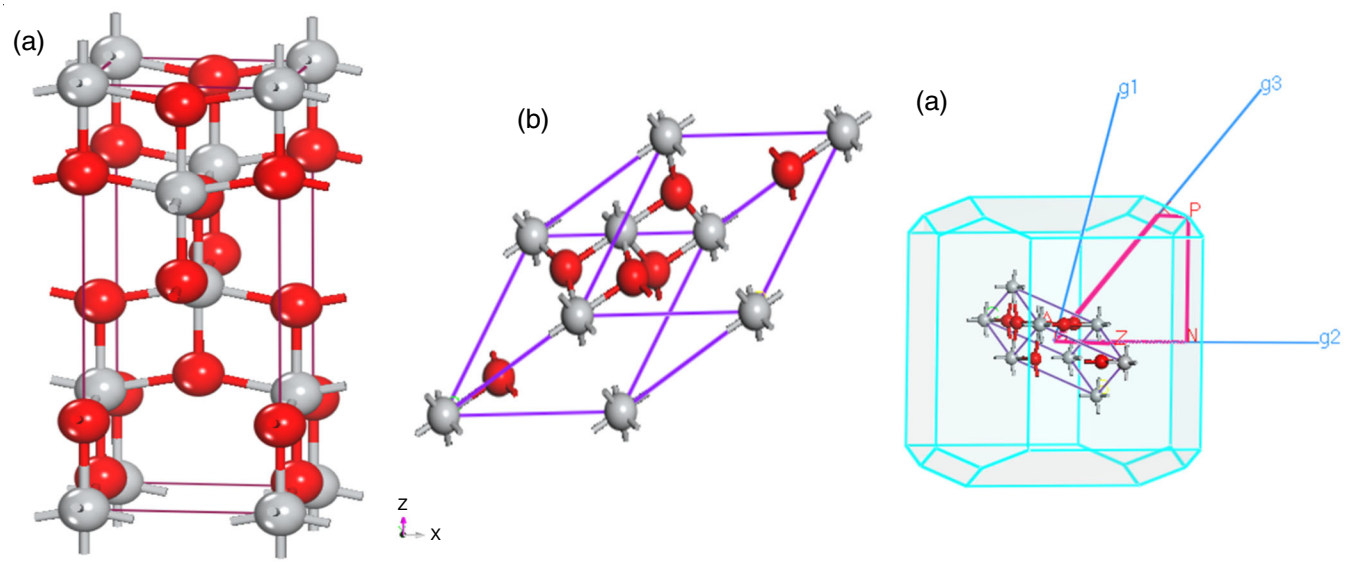

Fig. 1. DFT simulated TiO_2 anatase (a) unit cell in real space, (b) primitive unit cell and (c) unit cell in reciprocal space [12]

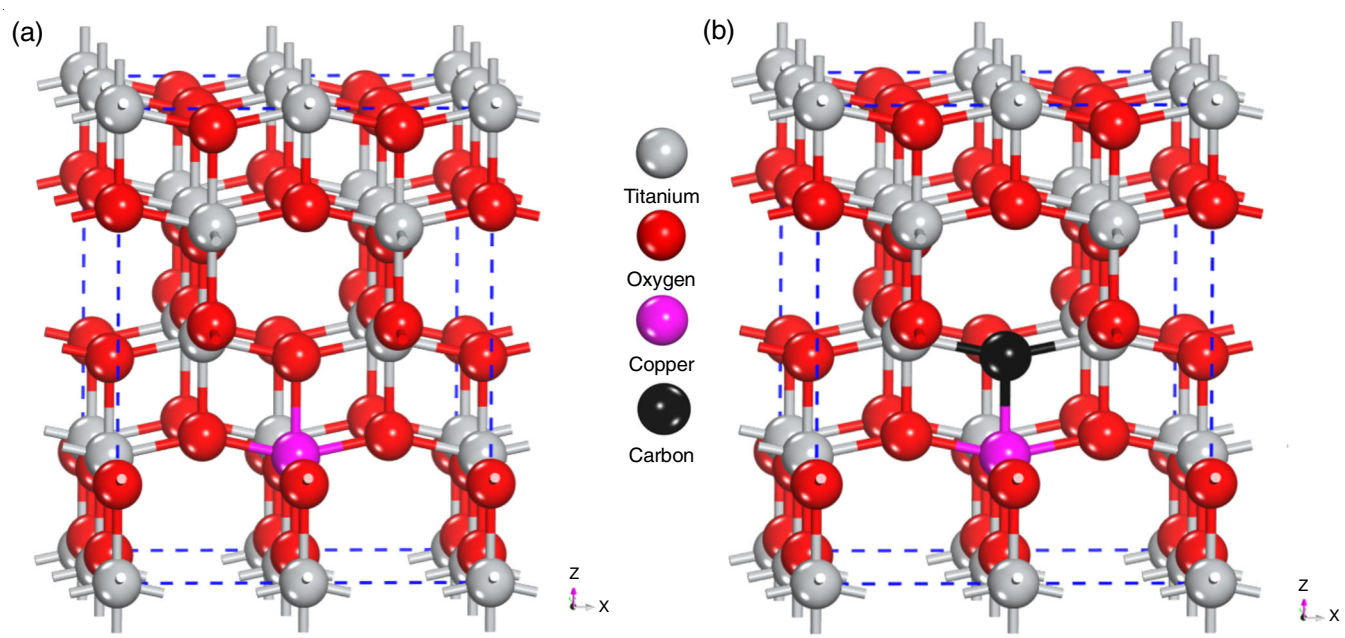

Fig. 2. The (2 × 3 × 1) TiO_2 anatase configured supercell models for the (a) Cu-doped and (b) C-Cu co-doped geometry

TABLE-1
COMPARISON OF THE OPTIMIZED LATTICE PARAMETERS OF THE DESIGNED MODELS

Cell parameters	Lattice parameters (Å)			Bond lengths (Å)			Band gap (eV)
	a (Å)	b (Å)	c (Å)	Ti-O	C-O	Cu-O	
Cu-doped TiO_2	3.789	3.789	9.532	1.946	–	1.959	2.47
C-Cu co-doped TiO_2	3.794	3.794	9.556	–	1.938	1.965	2.30
Exp Undoped TiO_2	3.785	3.785	9.539	1.914	–	–	3.20

atom with a Cu atom in the undoped TiO_2 anatase supercell model (Fig. 2b). For the Cu-doped TiO_2 systems, the lattice parameters $a = b = 3.789$ Å and $c = 9.532$ Å were simulated with the averaged Cu-O bond length (1.959 Å). For the C-Cu co-doped doped system, the optimized lattice parameters were $a = b = 3.794$ Å and $c = 9.556$ Å with the averaged C-O bond length (1.938 Å), shorter than the Ti–O bond length (1.946) and Cu-O (1.965 Å) greater than the Ti–O bond length [17,18]. The summarized different structure optimization parameters of the simulated undoped and C-Cu co-doped systems is given in Table-1.

Electronic structure: The electronic structure of a photocatalyst greatly influence the photocatalytic performance of the photocatalyst. Fig. 3 portrays the electronic band structure plots of the Cu and C-Cu co-doped TiO_2 models to have a deep understanding of the electronic structure and to choose the better dopants and better strategy to enhance the photocatalytic activity of the semiconductor photocatalyst. The Fermi energy level at zero-point energy was characterized with the black dashed line. The red colour was chosen for the VB states and the violet colour was chosen for the CB states. The simulated bandgap energy of the Cu-doped TiO_2 anatase model was 2.47 eV in comparison to 3.13 eV [12] of pure TiO_2 (Fig. 3a). The computed bandgap energy with GGA + U functionals (U = 8.47 eV) thus provided the bandgap energy calculation more reliable [12,18]. For the C-Cu co-doped TiO_2 anatase model, the dopant atoms' insertion into the TiO_2 lattice results in the structural distortions to modify the electronic structures. New impurity states were appeared in the bandgap region that caused significant changes in the electronic structure and thus reduced the bandgap energy [14,19]. The bandgap of C-Cu co-doped TiO_2 anatase model was narrowed down to 2.30 eV with the conduction band minima (CBM) moved in the direction of Fermi energy level to result in an effective bandgap reduction of TiO_2 anatase model. The increased number of electronic states was due to the insertion of C and Cu doped impurity states in the bandgap region, as was displayed in the band structure plots. As the result displayed, more bandgap energy reduction (~ 2.30 eV) was observed for C-Cu co-doped TiO_2 model. Therefore, this makes the electron excitation easier from VB to CB by absorbing less energetic visible light photons, thus ultimately enhance the optical absorption capability of the doped photocatalyst [20].

Density of states analysis: To examine the mechanism of the structural changes upon the electronic structure of the Cu-doped and C-Cu co-doped TiO_2 semiconductor, the TDOS and PDOS analysis were performed. The plots explored the fundamental effect of C, Cu dopants upon the electronic structure to develop an effective doped TiO_2 anatase configured model. The PDOS plot of Cu-doped TiO_2 in Fig. 4a demonstrated that the VB of the Cu-doped TiO_2 anatase model owned O2p + Cu2p hybrid states with fewer Ti3d + Cu3d states, whereas the CB owned more Ti3d + Cu3d states with fewer O2p + Cu2p states. The forbidden gap above the Fermi energy level at 0 eV was positioned up to ~ 2.47 eV and thus verifying the band structure analysis for the bandgap energy calculation about 2.47 eV of Cu-doped TiO_2 model. For C-Cu co-doped model, the bandgap energy was reduced more efficiently. The VB of the co-doped model adjusted the Ti2p, C2p and Cu2p hybridized states within the VB bandwidth from

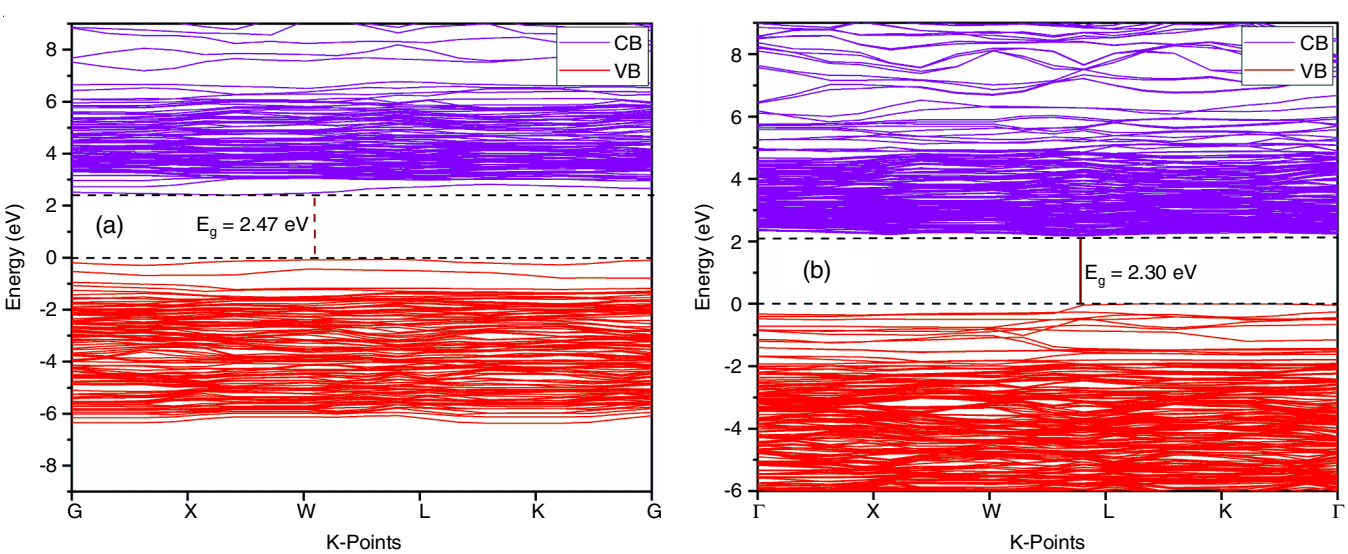

Fig. 3. DFT computed band structure projections of the (a) undoped and (b) C-Cu co-doped TiO_2 anatase models

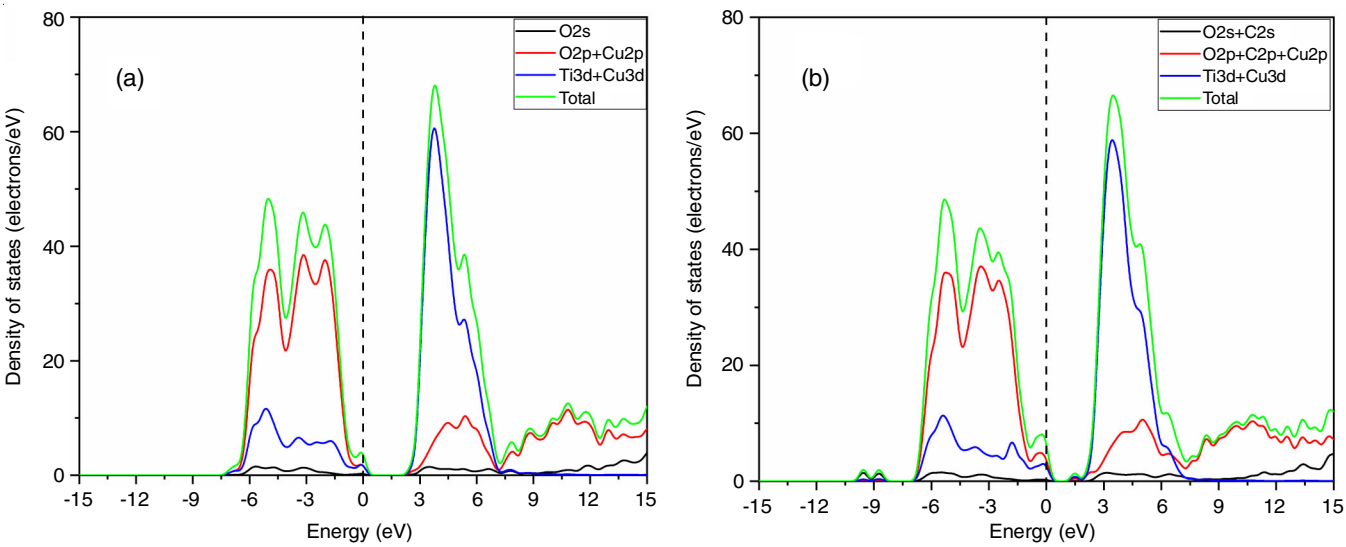

Fig. 4. Projected TDOS and PDOS *via* theoretical calculation for the (a) undoped and (b) C-Cu co-doped TiO_2 anatase models

-3 to -4 eV, whereas the CB region adopted the hybridized Ti 3*d* and Cu 3*d* states. The peak intensities of the energy states were thus signified due to the hybridization of these states. The enhanced peak intensities specify the increased amount of the induced impurity states from the insertion of the C-Cu co-dopants. The insertion of dopant impurity states at the top of valence band edge and bottom of the conduction band edge thus narrows down the bandgap to a value of 2.30 eV. Narrowing the bandgap reduces the electron's excitation energy available in the valence band to easily excite into the impurity states and subsequently to the conduction band too [21,22]. The required electron transition energy thus decreased for the C-Cu co-doped TiO_2 material to extend the optical absorption edge towards the visible light range. Therefore, the C-Cu co-doped model absorbs a greater number of visible energy photons and thus the photocatalytic activity might enhance strongly. Overall, the (C, Cu) co-doping vintages the best configuration of the band structure in terms of the bandgap and potential optical catalysis.

Optical properties: The electronic band structure modification of a photocatalyst can significantly affect the optical characteristics of a designed material due to the induction of the impurity atoms. The optical absorption spectra of Cu mono-doped and C-Cu co-doped TiO_2 anatase models are shown in Fig. 5. The simulated optical spectra of undoped TiO_2 anatase model predominantly corresponds to the UV radiation of the solar spectrum in the wavelength region between 200-380 nm due to their wide bandgap energy and meager visible light absorption thus limited the wider application range of TiO_2 photocatalyst as reported earlier [23,24]. The electronic band structure modifications alter the optical characteristics of the designed C, Cu co-doped TiO_2 models. On the other hand, for C-Cu co-doped TiO_2 anatase model, the resulting redshift of the optical absorption edge is ascribed to the changes in the electronic structure after dopants integration. The redshift in the absorption edge of C-Cu co-doped TiO_2 model was up to 515 nm due to an effective reduction of band-gap up to 2.30 eV. The combined effect of the addition of C and Cu impurity

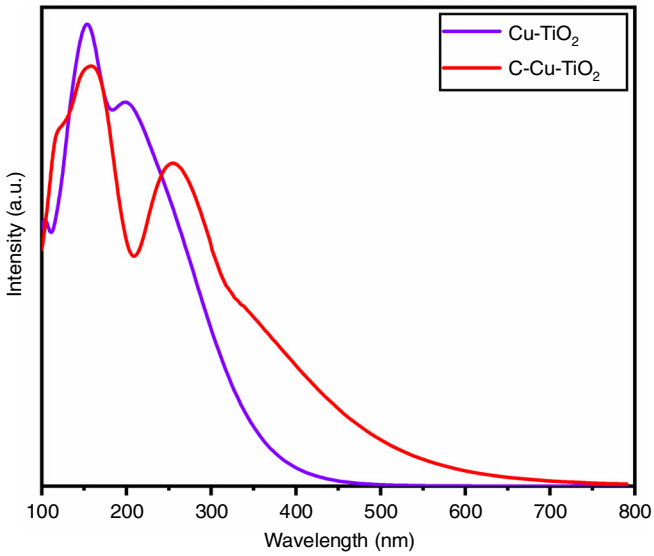

Fig. 5. Simulated combined absorption spectra of the TiO_2 and C-Cu-TiO_2 anatase models

states significantly reduced the bandgap energy and hence decreased the amount of energy required for the electron excitation, which efficiently improved the visible light absorption of TiO_2 photocatalyst. The results are also consistent with the band structure analysis, having a significant bandgap narrowing, that results in an easier transition of electrons from VB to the CB in the co-doped TiO_2 model than that occurs in the undoped and Cu-doped TiO_2 anatase models. Therefore, an enhanced visible energy absorption more positively affects the photocatalytic performance of TiO_2 photocatalyst.

Conclusion

The present study investigated the effect of Cu mono-doping and C-Cu co-doping on the structural, electronic and optical properties of TiO_2 anatase model *via* DFT calculations. The conventional GGA + PBE technique was adopted for the structural properties' calculations while the GGA + PBE + U technique was employed to find out the electronic and optical

properties of the designed undoped and doped TiO_2 anatase model. The bandgap energy of Cu-doped TiO_2 anatase model was examined around 2.47 eV with Hubbard's U valued ~ 8.47 eV. For the C-Cu co-doped TiO_2 models, the bandgap energies were significantly reduced as estimated ~ 2.30 eV in comparison to 3.13 eV of undoped TiO_2 model. The optical absorption edge of C-Cu co-doped model redshifted significantly due to the more bandgap reduction and thus improving the visible light absorption. The computed results inferred that the C, Cu dopants induce new impurity energy states in the band structure of TiO_2 anatase model to effectively narrow down the bandgap and absorb more visible light. Overall, the C-Cu co-doping of TiO_2 anatase photocatalyst improve the photocatalytic activity efficiently through visible solar light absorption and thus appeared a prominent option for the TiO_2 based photocatalytic water splitting technique.

ACKNOWLEDGEMENTS

The authors are thankful to Universiti Teknologi PETRONAS (UTP) and the ministry of higher education (MOHE) Malaysia for the Fundamental Research Grant Scheme (FRGS) (Grant No. FRGS/1/2019/STG07/UTP/01/1) to support this work financially.

CONFLICT OF INTEREST

The authors declare that there is no conflict of interests regarding the publication of this article.

REFERENCES

1. S. Sharma, S. Agarwal and A. Jain, *Energies*, **14**, 7389 (2021); https://doi.org/10.3390/en14217389
2. H. Ge, F. Xu, B. Cheng, J. Yu and W. Ho, *ChemCatChem*, **11**, 6301 (2019); https://doi.org/10.1002/cctc.201901486
3. A. Fujishima and K. Honda, *Nature*, **238**, 37 (1972); https://doi.org/10.1038/238037a0
4. M. Rafique, Y. Shuai and M. Hassan, *J. Mol. Struct.*, **1142**, 11 (2017); https://doi.org/10.1016/j.molstruc.2017.04.045
5. S. Piskunov, O. Lisovski, J. Begens, D. Bocharov, Y.F. Zhukovskii, M. Wessel and E. Spohr, *J. Phys. Chem. C*, **119**, 18686 (2015); https://doi.org/10.1021/acs.jpcc.5b03691
6. R. Singh and S. Dutta, *Fuel*, **220**, 607 (2018); https://doi.org/10.1016/j.fuel.2018.02.068
7. Y. Li, L. Ding, Z. Liang, Y. Xue, H. Cui and J. Tian, *Chem. Eng. J.*, **383**, 123178 (2020); https://doi.org/10.1016/j.cej.2019.123178,
8. F. He, A. Meng, B. Cheng, W. Ho and J. Yu, *Chin. J. Catal.*, **41**, 9 (2020); https://doi.org/10.1016/S1872-2067(19)63382-6
9. X. Dan, K.L. Yao, G.Y. Gao and L. Yang, *J. Magn.*, **335**, 118 (2013); https://doi.org/10.1016/j.jmmm.2013.02.010
10. T. Yun, F. Qing, D. Shoubing, L. Tong, G. Jiemei and W. Fang, *Acta Opt. Sin.*, **33**, 0816004 (2013); https://doi.org/10.3788/AOS201333.0816004
11. X. Yu, C. Li, H. Tang, Y. Ling, T.-A. Tang, Q. Wu and J. Kong, *Comput. Mater. Sci.*, **49**, 430 (2010); https://doi.org/10.1016/j.commatsci.2010.05.034
12. N.M. Mohamed, F. Ullah, R. Bashiri, C.F. Kait, M.S.M. Saheed and M.U. Shahid, In: Proceedings of the 6th International Conference on Fundamental and Applied Sciences, Springer, pp. 371-381 (2021).
13. F. Ullah, N.M. Mohamed, C.F. Kait, U. Ghani and M.S.M. Saheed, *Surf. Interfaces*, **30**, 101952 (2022); https://doi.org/10.1016/j.surfin.2022.101952
14. N. Tancogne-Dejean, M.A. Sentef and A. Rubio, *Phys. Rev. Lett.*, **121**, 097402 (2018); https://doi.org/10.1103/PhysRevLett.121.097402
15. M. Mesbahi and M.L. Benkhedir, *UPB Sci. Bull., Series A*, **79**, 293 (2017).
16. J. He, Q. Liu, Z. Sun, W. Yan, G. Zhang, Z. Qi, P. Xu, Z. Wu and S. Wei, *J. Phys. Chem. C*, **114**, 6035 (2010); https://doi.org/10.1021/jp911267m
17. J. Ananpattarachai, Y. Boonto and P. Kajitvichyanukul, *Environ. Sci. Pollut. Res. Int.*, **23**, 4111 (2016); https://doi.org/10.1007/s11356-015-4775-1
18. S.J. Clark, M.D. Segall, C.J. Pickard, P.J. Hasnip, M.I. Probert, K. Refson and M.C. Payne, *Z. Kristallogr. Cryst. Mater.*, **220**, 567 (2005); https://doi.org/10.1524/zkri.220.5.567.65075
19. J.G. Lee, Computational Materials Science: An Introduction, CRC Press (2016).
20. A. Chanda, S.R. Joshi, V.R. Akshay, S. Varma, J. Singh, M. Vasundhara and P. Shukla, *Appl. Surf. Sci.*, **536**, 147830 (2021); https://doi.org/10.1016/j.apsusc.2020.147830
21. F. Nunzi, F. De Angelis and A. Selloni, *J. Phys. Chem. Lett.*, **7**, 3597 (2016); https://doi.org/10.1021/acs.jpclett.6b01517
22. S.S. Nishat, M.J. Hossain, F.E. Mullick, A. Kabir, S. Chowdhury, S. Islam and M. Hossain, *J. Phys. Chem. C*, **125**, 13158 (2021); https://doi.org/10.1021/acs.jpcc.1c02302
23. Y.-H. Lin, H.-T. Hsueh, C.-W. Chang and H. Chu, *Appl. Catal. B*, **199**, 1 (2016); https://doi.org/10.1016/j.apcatb.2016.06.024
24. B. Liu and X. Zhao, *Appl. Surf. Sci.*, **399**, 654 (2017); https://doi.org/10.1016/j.apsusc.2016.12.075